Acta Materialia 227 (2022) 117685

Contents lists available at ScienceDirect

Acta Materialia

journal homepage: www.elsevier.com/locate/actamat

Full length article

Heterointerface and grain boundary energies, and their influence on microstructure in multiphase ceramics

Komal Syed[a], Nadjia B. Motley[a], William J. Bowman[a,b,*]

[a] Department of Materials Science & Engineering, University of California, Irvine, CA, United States
[b] Irvine Materials Research Institute, University of California, Irvine, CA, United States

ARTICLE INFO

Article history:
Received 27 December 2021
Revised 17 January 2022
Accepted 23 January 2022
Available online 24 January 2022

Keywords:
Multiphase ceramics
Grain boundary energy
Heterointerfaces
Atomic force microscopy
Faceting

ABSTRACT

Heterointerface energy measurements for multiphase systems are rarely reported in the scientific literature in contrast to grain boundary energies for single phase systems. Hence, thermal groove dimensions on the surfaces of single-phase (YSZ, Al_2O_3, $MgAl_2O_4$), two-phase (YSZ/$MgAl_2O_4$, YSZ/Al_2O_3), and three-phase (YSZ/$MgAl_2O_4$/Al_2O_3) ceramics were measured using atomic force microscopy to calculate relative energies for six different types of interfaces. Average grain boundary and interfacial energies were estimated from relative values calculated using previously published surface energies. Our results show that relative areas of interfaces in a multiphase composite are governed by relative interface energies. We show that Al_2O_3-Al_2O_3 homointerfaces occur less frequently in the multiphase systems studied, attributed to their higher grain boundary energies compared to YSZ-YSZ and $MgAl_2O_4$-$MgAl_2O_4$ boundaries. Using the complex three-phase ceramic system as a model, we also show that heterointerface energies are intermediate between the grain boundary energies of each of the two associated phases. Grain boundary and heterointerface energies for any specific type of boundary were similar for single phases versus multiphases, but the influence of grain boundary chemistry variations is reflected in the energy distribution. Our findings contribute novel insights on grain boundary and heterointerface energies that can inform materials design due to their strong influences on microstructural evolution.

1. Introduction

Grain boundaries and heterointerfaces are defects that have excess free energy per unit area. This excess energy of grain boundaries is a driving force for grain growth and thus plays an important role in microstructural development [1–4]. Several factors can affect grain boundary energy such as changes in temperature, grain boundary chemistry, etc. The effect of temperature on grain boundary energy has been studied in both pure and doped materials [3–7]. Typically, grain boundary energy decreases with increasing temperature in pure materials due to entropy [4,5,8]. However, grain boundary energy variation will also depend on changes in grain boundary chemistry for systems with solute/dopant segregation. For instance, Kelly et al. [5] showed that grain boundary energy increases with increase in temperature in Y-doped alumina samples. This is because bulk solubility generally increases with increase in temperature so interfacial segregants can dissolve back in the bulk (i.e., in the grains), resulting in the reduction of grain boundary excess.

While there is a substantial number of studies on segregation to grain boundaries in single-phase ceramics with or without dopants [5,9–19], our recent literature review [20] found a clear lack of work on polycrystalline ceramic heterointerfaces. Single-phase studies are useful to understand grain boundary properties in model and relatively simple systems. However, engineering ceramics are often (intentionally or not) multi-phase with much more interface diversity. Our recent study [21] on a three-phase ceramic system has shown that elemental segregation behavior can differ depending on sample composition. Furthermore, that work also highlighted that while some interfaces showed segregation, others did not. Since grain boundary segregation is expected to affect grain boundary energy, it is thus important to extend grain boundary energy analysis to heterointerfaces in multi-phase systems. There is, however, a lack of literature on energy measurements for heterointerfaces due to the complexity of multi-phase systems and several assumptions involved for such calculations. There have only been a handful of studies (~<10 per our knowl-

* Corresponding author.
E-mail addresses: KSYED1@UCI.EDU (K. Syed), nmotley@uci.edu (N.B. Motley), will.bowman@uci.edu (W.J. Bowman).

https://doi.org/10.1016/j.actamat.2022.117685

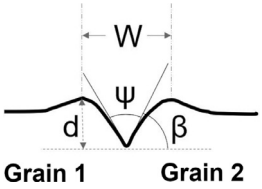

Fig. 1. Schematic of a thermal groove defining depth (d), total groove width (W), and angles β and ψ.

edge) conducted previously in which multiphase samples were analyzed for grain boundary and heterointerface energy measurements [1,8,22,23].

The most common way to measure grain boundary energy experimentally is by observing the groove geometry of interfaces, which are assumed to be in thermodynamic equilibrium [1,8,24]. When a polished surface is thermally etched, atoms/ions near the interface are preferentially removed or relocated, forming grooves at interface junctions, Fig. 1. The geometry of a groove can be used to measure the ratio of grain boundary energy to surface energy:

$$\frac{Y_{GB}}{Y_S} = 2\ \sin\beta = 2\ \cos\frac{\psi}{2} \tag{1}$$

where, $Y_{GB}$is grain boundary energy, Y_S is surface energy, β is groove angle and ψ is dihedral angle as shown in Fig. 1. The relative grain boundary energy (Y_{GB}/Y_S) can be calculated using the relationship between β and groove depth and width as given by Mullins [25]:

$$\tan\beta = 4.73\ \frac{d}{W} \tag{2}$$

While the influence of grain boundary energies on microstructural development is well-established in single phase polycrystals, the purpose of this paper is to test the hypothesis that relative interface areas in multiphase polycrystalline systems are governed by relative interface energies. Since most of the previous work on grain boundary energies in ceramics has been performed on undoped/doped single phase systems, our study will focus primarily on 2-phase and 3-phase multiphase systems, while also using single-phase materials for proof of concept and comparison to previous literature. The hypothesis is tested by analyzing thermal grooves using atomic force microscopy (AFM) to measure the relative (and absolute energies) of interfaces in single phase (YSZ, Al_2O_3, and $MgAl_2O_4$), 2-phase (YSZ/Al_2O_3, YSZ/$MgAl_2O_4$, and Al_2O_3/$MgAl_2O_4$) and 3-phase (YSZ/Al_2O_3/$MgAl_2O_4$) ceramic systems. The overall goal of this study is thus to analyze how interface energies specifically affect microstructural evolution in multiphase polycrystalline systems.

2. Materials and methods

Starting powders of 8 mol% yttria stabilized zirconia or YSZ ($Y_{0.08}Zr_{0.92}O_2$, TZ-8YS Tosoh), Al_2O_3 (TM-DAR Taimei) and $MgAl_2O_4$ (S30CR Baikowski) were used to make single phase, 2-phase (equal volume 50%) and 3-phase (equal volume 33%) ceramics. The single-phase systems are YSZ, $MgAl_2O_4$ (spinel) and Al_2O_3 (alumina). The two-phase systems include YSZ/$MgAl_2O_4$, YSZ/Al_2O_3 and $MgAl_2O_4$/Al_2O_3, while the three-phase system is YSZ/$MgAl_2O_4$/Al_2O_3. The powders were attrition milled for ~8 h at 600 rpm with isopropyl alcohol in a Teflon-coated tank. The resulting slurry was dried overnight at 100 °C. Mortar and pestle were used to break any agglomerates before sieving the dried slurry to 106 μm. The mixed powder was uniaxially pressed, via a carver press, at 22 kpsi for 5 min into cylindrical shaped samples with a green body density of 54 ± 2%. Single phase and 2-phase green body samples were sintered at 1550 °C for 10 h in air with heating rate of 10 °C/min, while 3-phase sample was sintered at 1550 °C for 20 h. Sintered samples were polished to 0.05 μm finish.

After sintering, the pellets were subjected to thermal etching in a tube furnace. Initial thermal etching was conducted at 1500 °C for 3 h using heating rate of 10 °C/min and cooling rate of 20 °C/min. This high temperature and relatively long time was selected to achieve wide grooves to minimize error associated with AFM tip geometry. However, due to severe faceting behavior in some spinel-based compositions, the etching temperature and time had to be adjusted to minimize faceting. However, low temperatures result in shallow grooves and can also make it difficult to characterize heterointerfaces due to preferential etching behavior of different phases so not all samples could be etched at the lower temperatures. Thermal etching treatments for the following samples had to be adjusted below 1500 °C: single-phase spinel (1300 °C for 15 min) and 3-phase samples (1450 °C for 1 h). Spinel/alumina system showed the most severe faceting behavior, and several thermal treatments were attempted. However, due to the experimental challenges in characterizing spinel/alumina heterointerfaces, this system was removed from the grain boundary energy analysis. The details of these experimental challenges can be found in the supplementary information.

The geometry of thermal grooves was characterized using AFM in tapping mode. Topographic maps were collected using Anton-Paar Tosca AFM. Silicon tips used for AFM measurements had 30 nm thick aluminum reflex coating on the detector side of cantilever (Arrow-NCR, Nanoworld, Neuchatel, Switzerland). The tips had a radius <10 nm, force constant of 42 N/m and resonance frequency of 285 kHz.

Grain boundaries and heterointerfaces were selected from random locations on sample surface. To differentiate between the different phases of multiphase samples in AFM, SEM images were taken first from random areas on sample and then the same areas were then mapped in AFM to measure the interfacial energies. Line profiles were drawn perpendicular across each boundary, and width (w) and depth (d) values were extracted from each side of the groove to measure relative grain boundary energy using similar procedure as described in previous studies [5,11] (see Fig. 2). The depth and width values were measured using Gwyddion software and ratio of grain boundary to surface energy was calculated using Eq. (3):

$$\frac{Y_{GB}}{Y_S} = 2\sin\left(\tan^{-1}\left(m\left(\frac{d}{2w}\right)\right)\right) \tag{3}$$

This relation is based on the Mullins analysis [25]. 'm' is typically considered a constant equal to 4.73 (as shown in Eq. (2)) but this value can deviate when w/d ratio becomes smaller, so a correction was applied to m using the known relationship between m and w/d [5,26].

While Eq. (3) is a common method to measure relative grain boundary energies, it is based on several assumptions. For instance, (1) it assumes that the grain boundary is normal to the surface, (2) the two surface energies (on either side of groove) are the same and (3) that surface energy anisotropy is small enough to be ignored [19]. While recognizing that one specific value of relative interfacial energy derived from one grain boundary is not useful by itself, many authors have pointed out that the analysis of many grain boundaries using this method can result in meaningful average values and provide useful grain boundary energy distributions [1,5,11,14,19,27].

Error from the radius of curvature of the AFM tip can introduce artifacts and limit the accuracy of groove geometry measurements. A groove width many times larger than the radius of curvature of AFM tip should decrease such error in groove measurements. Saylor and Rohrer [14] previously detailed a method to estimate this

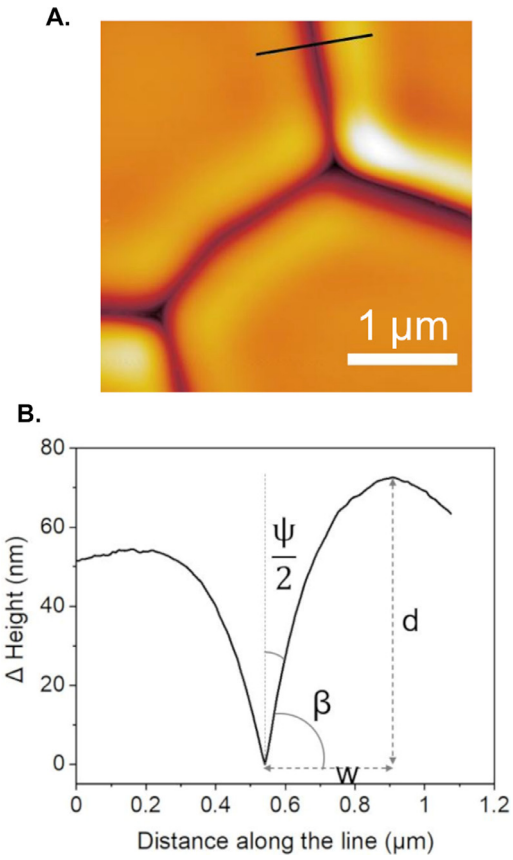

Fig. 2. (A) Representative AFM image of YSZ surface after thermal etching at 1500 °C. (B) Line profile across YSZ-YSZ grain boundary showing 'd' and 'w' used to measure relative grain boundary energy.

error depending on the groove width and groove angle β. Application of this method has found that for groove widths >1 μm, the probe size has minimal to no effect on measurements [5]. This correction method was originally calculated for an AFM tip of 60 nm radius of curvature, but the more current AFM tips used in this study have <10 nm radius of curvature, so even smaller groove widths should be able to be accurately measured. It should be noted that while tip correction can be important, the error due to finite probe size is systematic and does not change the relative data [11,22]. Considering this, AFM tip correction has been ignored in our study.

2.1. Grain boundary energy analysis for homointerfaces

Since the groove profiles are usually asymmetric (Fig. 2), even between two same phase grains, each side of the groove was considered separately to measure relative grain boundary energy. This implies that two grain boundary energy values were calculated for each side as if they were two symmetric grooves. 45–72 homointerfaces of each kind (YSZ-YSZ, alumina-alumina, spinel-spinel) were characterized for the different samples in this study. The relative grain boundary energies of YSZ-YSZ, alumina-alumina, spinel-spinel grain boundaries were multiplied by reported average Υ_S values for YSZ, alumina or spinel respectively (see Table 2) to obtain average Υ_{GB} values for this study.

2.2. Interfacial energy analysis for heterointerfaces

Eq. (3) has been mainly used in literature for analysis of homointerfaces. However, the simplified approach of considering each side of the groove separately can be used to estimate average interfacial energies for heterointerfaces also. First, we measured the relative grain boundary energy for each side of the groove (each side corresponds to a different phase) using respective depth and width values (Fig. 3). Then the calculated relative energy value for each side is multiplied by the respective average surface energy of that phase (Table 2). For example, the calculated relative energy for YSZ side of the groove in YSZ/Alumina heterointerface (Fig. 3B) is multiplied by 1.16 J/m^2 (Υ_{S1}) and the calculated relative energy for the Alumina side of the groove is multiplied by 2.64 (Υ_{S2}). The resulting values are estimated absolute energies which are then averaged to obtain the interfacial energy for the heterointerface, YSZ/Alumina in this example. We understand that this is an over-simplified way to estimate average interfacial energies; however, this allows for a way to compare the interfacial energies of homo- and hetero-interfaces. In the past studies, typically only the relative energies of each side of a grain boundary or heterointerface groove have been reported [22].

Table 1
Average grain sizes for single and multi-phase samples sintered at 1550 °C.

Material System	Average grain size (μm)
Single-phase	
YSZ	6.0 ± 2.2
Spinel	2.3 ± 1.1
Alumina	5.1 ± 2.4
2-phase	
YSZ/Alumina	0.8 ± 0.3 (YSZ)
	0.7 ± 0.2 (Alumina)
YSZ/Spinel	1.2 ± 0.3 (YSZ)
	1.3 ± 0.4 (Spinel)
3-phase	
YSZ/Spinel/Alumina	1.1 ± 0.3 (YSZ)
	1.5 ± 0.7 (Alumina)
	1.4 ± 0.4 (Spinel)

3. Results and discussion

3.1. Effects of similar thermal etching treatment on different compositions

SEM images of single phase, two-phase and three-phase samples thermally etched at 1500 °C are shown in Fig. 4. The grain sizes for all compositions are provided in Table 1. While alumina grains showed some surface faceting (Fig. 4B), spinel was found to be severely faceted with the 1500 °C thermal etching treatment (Fig. 4C). For accurate grain boundary measurements, both the temperature and time had to be reduced for spinel to 1300 °C for 15 min to minimize surface reconstruction. Faceting behavior in ceramics is not a novel concept and is known to occur in a number of different ceramic materials, including spinel [22,31–34]. However, it is interesting to note that the spinel grains in the YSZ/Spinel sample (Fig. 4D) did not show strong faceting unlike the single-phase spinel. Y and Zr have very low reported solubility in spinel [35,36], but segregation of Y/Zr to spinel surfaces can stabilize the surfaces against the strong surface reconstruction phenomenon observed in single-phase spinel. In the 3-phase system, there was also faceting observed for many of the spinel grains (as shown by red arrows in Fig. 4F) and temperature and time had to be adjusted to minimize faceting while also optimizing groove dimensions. Since the solubility of alumina in spinel increases with temperature [37], it is likely that the spinel grains are no-longer stoichiometric spinel in 3-phase sample but are rich in Al. However, the sample compositions after sintering were not determined for this study. We believe enhanced Al-solubility in spinel causes increase in surface reconstruction during the heating treatment and results in pronounced faceting behavior. This is most evident

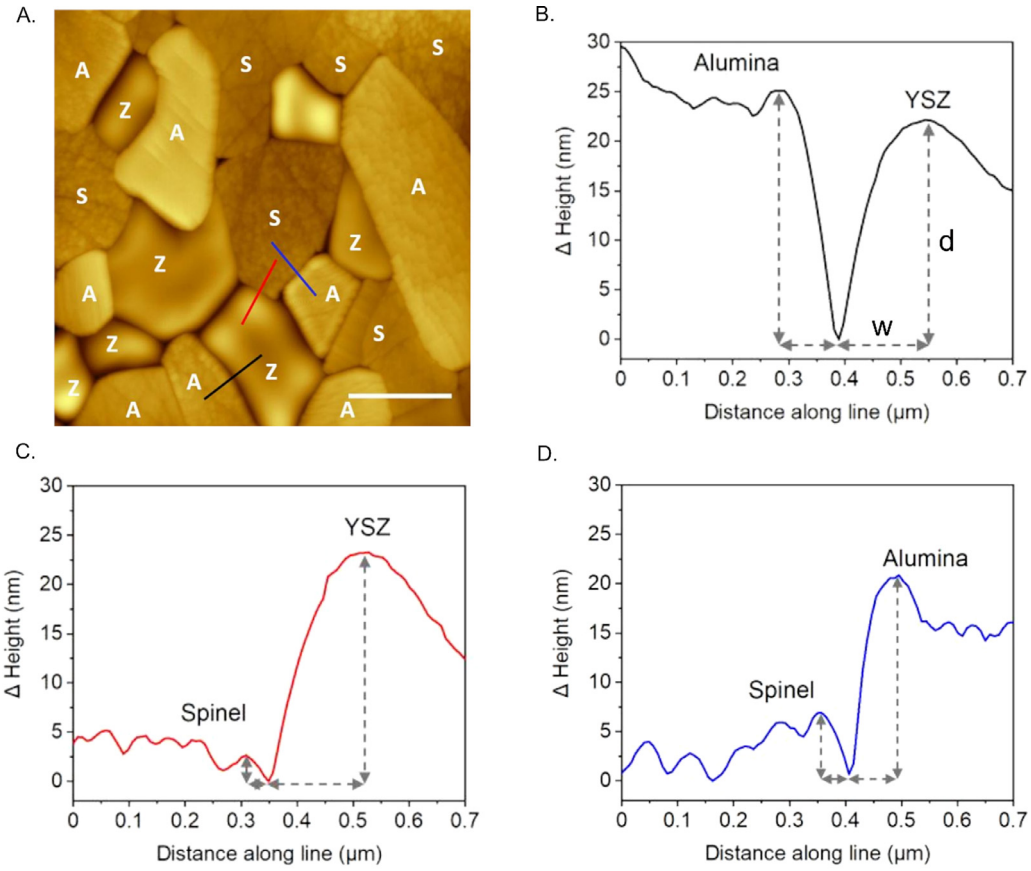

Fig. 3. (A) Representative AFM 2D topographical map of thermally etched 3-phase sample composed of YSZ/Spinel/Alumina. (B–D) Line profiles showing the groove profiles of the three types of heterointerfaces corresponding to similar colored lines drawn in (A): Alumina/YSZ, Spinel/YSZ and Spinel/Alumina, respectively.

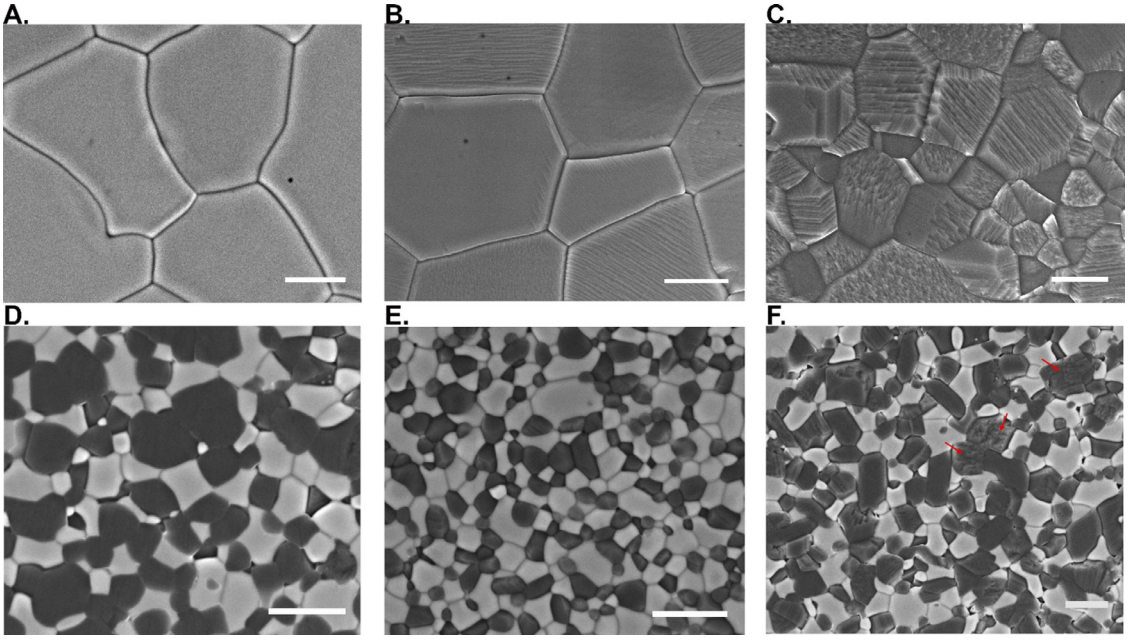

Fig. 4. SEM images of (A) YSZ, (B) Alumina, (C) Spinel, (D) YSZ/Spinel, (E) YSZ/Alumina, and (F) YSZ/Spinel/Alumina after thermal etching at 1500 °C. Scale bar is 2 μm. Red arrows in (F) indicate faceting in some spinel grains of 3-phase sample (For interpretation of the references to color in this figure legend, the reader is referred to the web version of this article.).

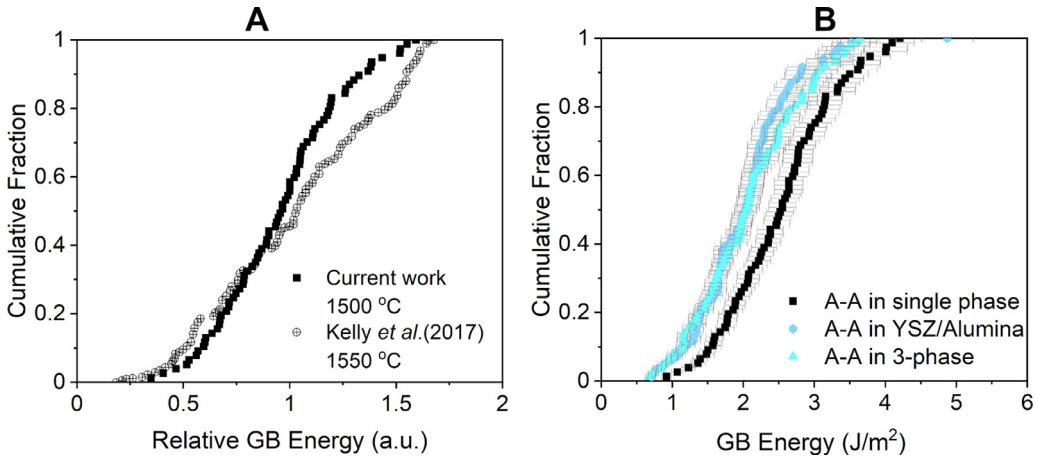

Fig. 5. (A) Cumulative distribution of relative grain boundary energies in single phase alumina compared to a previous study [5], (B) Cumulative distributions of average grain boundary energies for alumina-alumina (A-A) homo-interfaces in single phase alumina, two-phase (YSZ/Alumina) and three-phase (YSZ/Alumina/Spinel) samples thermally etched at 1500 °C.

Table 2
Reported surface energies at room temperature for polycrystalline YSZ, Al_2O_3 and $MgAl_2O_4$.

Sample	Average Surface Energy (J/m^2)
YSZ	1.16 ± 0.08 [28]
α-Al_2O_3	2.64 ± 0.2 [29]
$MgAl_2O_4$	1.65 ± 0.04 [30]

in the case of two-phase spinel/alumina (with no Y and Zr present; see Figs. S1 and S2), but also in 3-phase sample (to a lesser extent due to likely Y/Zr presence as discussed).

3.2. Grain boundary energies of homointerfaces in different compositions

Fig. 5A shows a cumulative distribution plot for all the characterized thermal grooves in single phase alumina sample etched at 1500 °C. The average *relative* grain boundary energies (Υ_{GB}/Υ_S) measured for the alumina sample is 1.0 ± 0.3. Our calculated average relative grain boundary energy is very similar to the reported values in literature. For alumina, Handwerker et al. [27] and Saylor and Rohrer [14] both measured relative energies to be 1.2 (at 1600 °C), Dillon et al. [11] reported 1.1 (at 1400 °C), and Kelly et al. [5] reported ~1.0 (1450 °C, 1550 °C, 1650 °C). Fig. 5A also shows the cumulative distribution plot for un-doped alumina thermally etched at 1550 °C from the published work of Kelly et al. [5] Some changes in relative energy distribution plots (Fig. 5A) are expected between different samples, difference in etching temperatures, and if AFM tip correction is applied to the data or not.

Fig. 5B suggests that average grain boundary energy in single phase alumina is slightly higher than the multi-phase samples (Table 3). Cumulative distribution curves of average grain boundary energies of alumina-alumina (A-A) homointerfaces, obtained by multiplying relative energies to reported surface energy of alumina (Table 2), in single phase, 2-phase and 3-phase samples. The shape of the distribution curve is almost the same for A-A grain boundaries in single phase, 2-phase and 3-phase samples; however, the energy distribution plots for YSZ/Alumina and 3-phase are slightly shifted to the left compared to the plot of single-phase alumina. The error bar associated with each data point in Fig. 5B reflects the propagated uncertainty obtained by multiplying relative energy with average surface energy and its standard deviation from Table 2. We believe this is because of changes in A-A grain boundary chemistry in multi-phase samples. We previously showed [21] that Y/Zr segregate to A-A grain boundaries in 3-phase sample same as this study. The segregation of Y and Zr to these grain boundaries in multi-phase samples would likely lower the grain boundary energies. While the variations in average energies of A-A grain boundaries are small between the three samples, the clear shift of the multi-phase energy distribution plots to the left (Fig. 5B) suggests segregation is likely responsible for lower grain boundary energies in general.

Unlike the shift seen in A-A distribution plots (Fig. 5B) between single and multi-phase samples, YSZ-YSZ (Z-Z) cumulative distribution plots do not show any significant difference between four different samples (Fig. 6A). The shape of the Z-Z energy distribution plots is almost the same for all samples shown in Fig. 6A: single phase YSZ, 2-phase YSZ/Spinel and YSZ/Alumina, and 3-phase sample. The average grain boundary energy for all four samples was calculated to be ~0.8–0.9 J/m^2 as shown in Table 3. This suggests that Z-Z grain boundary energies do not change much with varying samples. Tsoga and Nikolopoulos [18] measured average YSZ grain boundary energy to be ~0.6 J/m^2 using metal wetting technique. Costa et al. [28] reported grain boundary energies for 8, 10 and 12 mol% cubic YSZ to be ~0.9 ± 0.5 using calorimetric measurements. Thus, our measured average grain boundary energies for YSZ-YSZ homointerfaces match well to previously reported literature.

In pure/undoped YSZ, it is known that Y segregation occurs at the grain boundaries of single-phase YSZ [16,38–40]. However, this segregation behavior can differ when other phases are included in the system. Using energy dispersive X-ray spectroscopy, our previous work showed that Al segregation occurs instead of Y at YSZ-YSZ grain boundaries in a 3-phase ceramic composed of YSZ/Alumina/Spinel [21]. In both cases, segregation of Y or Al is accompanied by depletion of Zr [21,38]. Interestingly, the difference in ionic size between Al^{3+} and Zr^{4+} or Y^{3+} and Zr^{4+} is very similar (assuming same coordination) [41]. Based on the results of previous work, it is possible that there is no significant difference in grain boundary energies whether Y or Al segregation takes place at YSZ-YSZ grain boundaries. This would explain the results of our study showing similar average grain boundary energies of YSZ-YSZ homointerfaces in single phase, 2-phase and 3-phase systems (Table 3).

Different thermal etching treatments were performed for spinel (1300 °C; 15 min), YSZ/spinel (1500 °C; 3 h) and 3-phase (1450 °C; 1 h) samples to control faceting in spinel grains, and likely contributed to the different shapes of cumulative distribution plots for spinel-spinel boundaries (Fig. 6B). Faceting behavior in pure spinel

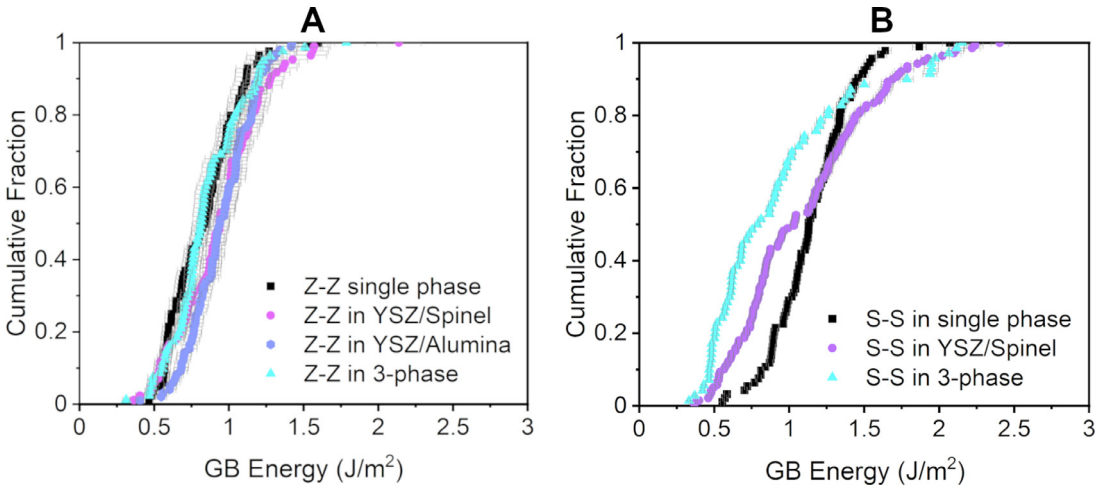

Fig. 6. (A) Cumulative distributions of average grain boundary energies for YSZ-YSZ (Z-Z) homo-interfaces in single phase YSZ, two-phase YSZ/Alumina and YSZ/Spinel, and three-phase YSZ/Alumina/Spinel samples, all thermally etched at 1500 °C. (B) Cumulative distributions of average grain boundary energies for Spinel-Spinel (S-S) homo-interfaces in single phase Spinel (1300 °C), two-phase YSZ/Spinel (1500 °C), and three-phase YSZ/Alumina/Spinel sample (1450 °C) thermally etched at different temperatures.

Table 3
Average grain boundary energies for interfaces in single and multi-phase systems.

Material Systems	GB Type	Etching Temperature (°C)	Average GB energy (J/m^2)
	Single phase		
YSZ	*YSZ-YSZ*	1500	0.8 ± 0.2
Spinel	*Spinel-Spinel*	1300	1.1 ± 0.3
Alumina	*Alumina-Alumina*	1500	2.5 ± 0.7
Two-phase			
YSZ/Alumina	*YSZ-YSZ*	1500	0.9 ± 0.2
	Alumina-Alumina	1500	2.0 ± 0.7
	YSZ-Alumina	1500	1.5 ± 0.4
YSZ/Spinel	*YSZ-YSZ*	1500	0.9 ± 0.3
	Spinel-Spinel	1500	1.1 ± 0.4
	YSZ-Spinel	1500	1.2 ± 0.3
Three-phase			
YSZ/Spinel/Alumina	*YSZ-YSZ*	1500	0.9 ± 0.3
	Alumina-Alumina	1500	2.1 ± 0.7
	YSZ-Alumina	1500	1.6 ± 0.5
	Spinel-Spinel	1450	0.9 ± 0.5
	Spinel-Alumina	1450	1.4 ± 0.5
	YSZ-Spinel	1450	0.9 ± 0.4

has been reported in previous studies also [31]. On average, the grain boundary energy of spinel-spinel homointerfaces was calculated to be 1.1 ± 0.3 J/m^2 in spinel sample, 1.1 ± 0.4 J/m^2 in YSZ/spinel sample, and 0.9 ± 0.5 J/m^2 in 3-phase sample. This is very similar to the reported value by Teevan [31] for undoped spinel (thermal etched at 1200 °C) of ~0.9 J/m^2 (when their reported relative grain boundary energy of 0.53 (γ_{GB}/γ_S) is multiplied by average surface energy for spinel, Table 2). While there is no considerable difference in average spinel grain boundary energies for the different samples shown in Table 3 (considering standard deviations), the shape of the distribution plots can provide us useful insights. The shape of the blue (triangular marker) and purple (circular marker) cumulative distribution plots in Fig. 6B are similar since the etching treatments were quite similar compared to the thermal etching for single-phase spinel (black curve). Spinel-spinel (S-S) thermal grooves were found to be narrower/shallower than other interfaces (Z-Z, A-A, Z-A, Z-S, A-S), so we expect the error associated with the finite size of AFM probe to be higher for the energy measurements in Fig. 6B. However, the etching temperatures are not very different, so the thermal groove geometry will be underestimated by likely the same amount and S-S grain boundaries can still be compared within different samples.

3.3. Energies of homointerfaces vs. heterointerfaces in three-phase ceramic

One of the major findings of this study is that the average energy of heterointerfaces is intermediate between the average grain boundary energies of the two phases that make up the heterointerface, and not distinctly higher even though the heterointerfaces have structural and chemical discontinuity. This result is consistent with Dillon et al. [22] who measured relative energies of heterointerfaces between doped aluminas and their equilibrium precipitates of spinel, silica, yttrium aluminum garnet, and calcium hexaluminate. Fig. 7 shows cumulative distribution plots for interfacial energies (J/m^2) for the three heterointerfaces, and for grain boundary energies (J/m^2) for the two phases associated with each heterointerface in the 3-phase sample. The AFM data for YSZ-YSZ, alumina-alumina and YSZ-alumina interfaces was collected after thermally etching the 3-phase sample at 1500 °C for 3 h. For the remaining three interfaces, spinel-spinel, spinel-alumina and YSZ-spinel, the etching temperature was lowered to 1450 °C for 1 h (after re-polishing) to reduce faceting in spinel grains. It would be ideal to lower the temperature even further to minimize surface reconstruction during heat treatment; however, spinel-spinel grooves

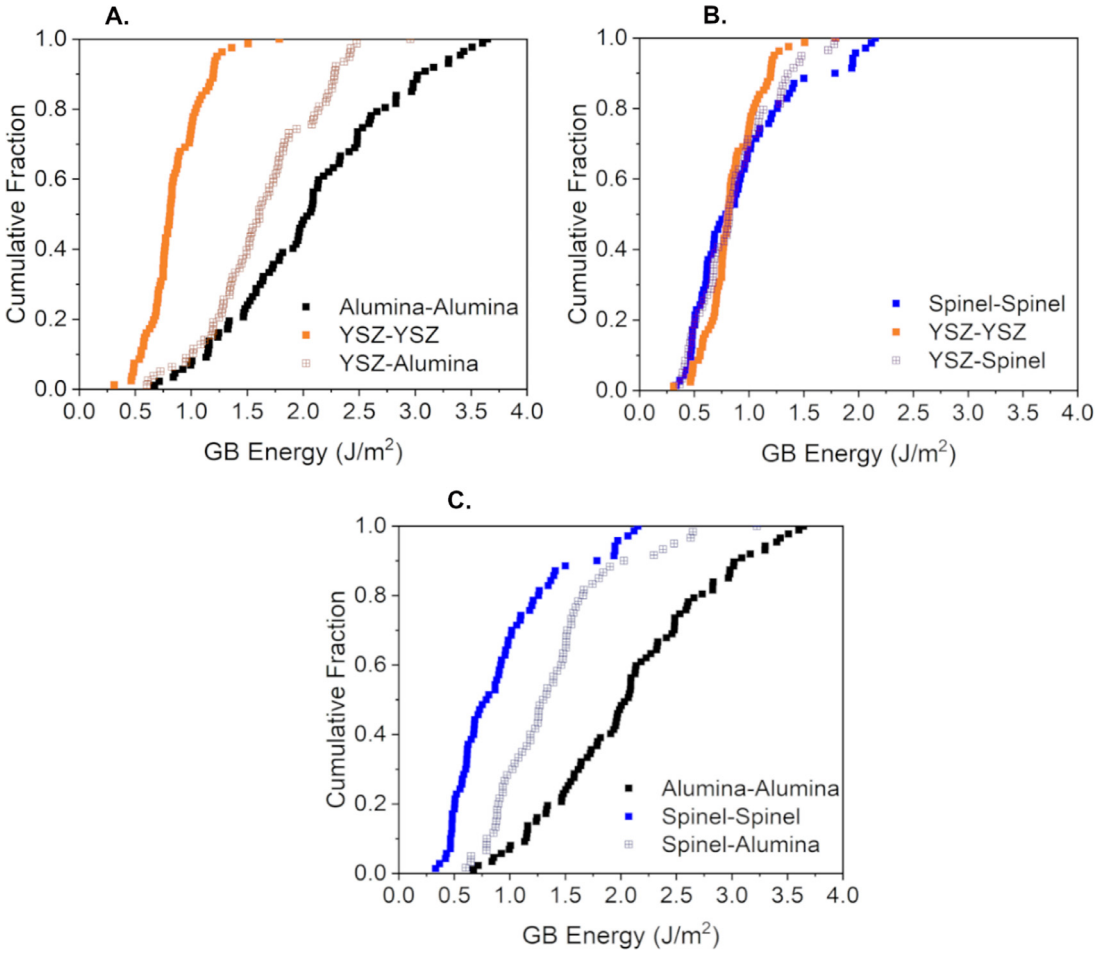

Fig. 7. (A) Cumulative energy distributions (CEDs) in a 3-phase sample. (A) CEDs of alumina-alumina, YSZ-YSZ grain boundaries and YSZ-alumina heterointerfaces. (B) Cumulative energy distributions of spinel-spinel, YSZ-YSZ grain boundaries and YSZ-spinel heterointerfaces in 3-phase sample. (C) Cumulative energy distribution of alumina-alumina, spinel-spinel grain boundaries and spinel-alumina heterointerfaces in 3-phase sample.

were found to be very shallow below 1400 °C as can also be observed in Fig. 3. Fig. 7A shows the cumulative distribution plot of YSZ-alumina interfacial energies to be intermediate between YSZ-YSZ and alumina-alumina grain boundary energies in 3-phase sample. Similarly, cumulative distribution plot for spinel-alumina is intermediate between alumina-alumina and spinel-spinel grain boundary energies (Fig. 7C). Since the grain boundary energies for YSZ-YSZ and spinel-spinel interfaces are quite similar, the cumulative distribution plot for YSZ-spinel is similar to energies of each of the two phases (Fig. 7B). The energy distributions for all the heterointerfaces in our study thus show that interfacial energies of interphase interfaces are not higher or lower than the respective constituent single phase grain boundary energies, but in fact are intermediate to the boundary energies of the two phases associated with the interface.

3.4. Influence of grain boundary and interfacial energies on microstructural evolution in multiphase systems

To better understand the role of grain boundary energies on microstructural evolution, we focused on our 2-phase samples. First, a theoretical arrangement of a 2-phase system (equal grain size) was used to calculate grain boundary length fractions for homo- and hetero-interfaces in an ideally random system (Fig. 8). For random situations, the fraction of each of the homointerfaces is ~25%, while for the heterointerfaces ~50%. We evaluated how the grain boundary length fractions differ in our actual samples. The calculated length fractions through two-dimensional surface analysis will thus provide us critical insights on how relative interface areas in three-dimensional system are affected by relative interface energies in multiphase systems. We calculated the length fraction of each type of interface/grain boundary from random regions in YSZ/spinel and YSZ/alumina samples that were structurally homogeneous. Representative regions of each of these 2-phase samples are shown in Fig. 8. For YSZ/alumina, 18.7% grain boundaries were Z-Z, 12.2% were A-A, and 69.1% were Z-A (Fig. 8); all measured for a region ~20 μm x 15 μm. These calculations show that there are less alumina-alumina grain boundaries than YSZ-YSZ grain boundaries, while A-Z heterointerfaces are in majority. The average grain boundary energy for Z-Z is 0.9 ± 0.2 J/m^2, A-A is 2.0 ± 0.7 J/m^2, and Z-A is 1.5 ± 0.4 J/m^2 (Table 3). Since the calculated average interfacial energy for A-A boundaries is higher than Z-Z boundaries in YSZ/Alumina sample, it would suggest that the system reduces the number of A-A boundaries during sintering to lower the overall system energy. The elimination of A-A boundaries can occur via grain growth. This matches well with our grain boundary fraction calculations (Fig. 8), with lower grain boundary length fractions of A-A boundaries than Z-Z boundaries. This implies that the relative interface area of A-A is lower than Z-Z in YSZ/alumina system because of higher average energy of A-A interfaces compared to Z-Z interfaces. However, it is difficult to correlate average Z-A interfacial energy with the fraction of Z-A interfaces in the experimental microstructure. Unlike the homointerfaces which can be eliminated by grain growth to minimize energy of the system, heteroin-

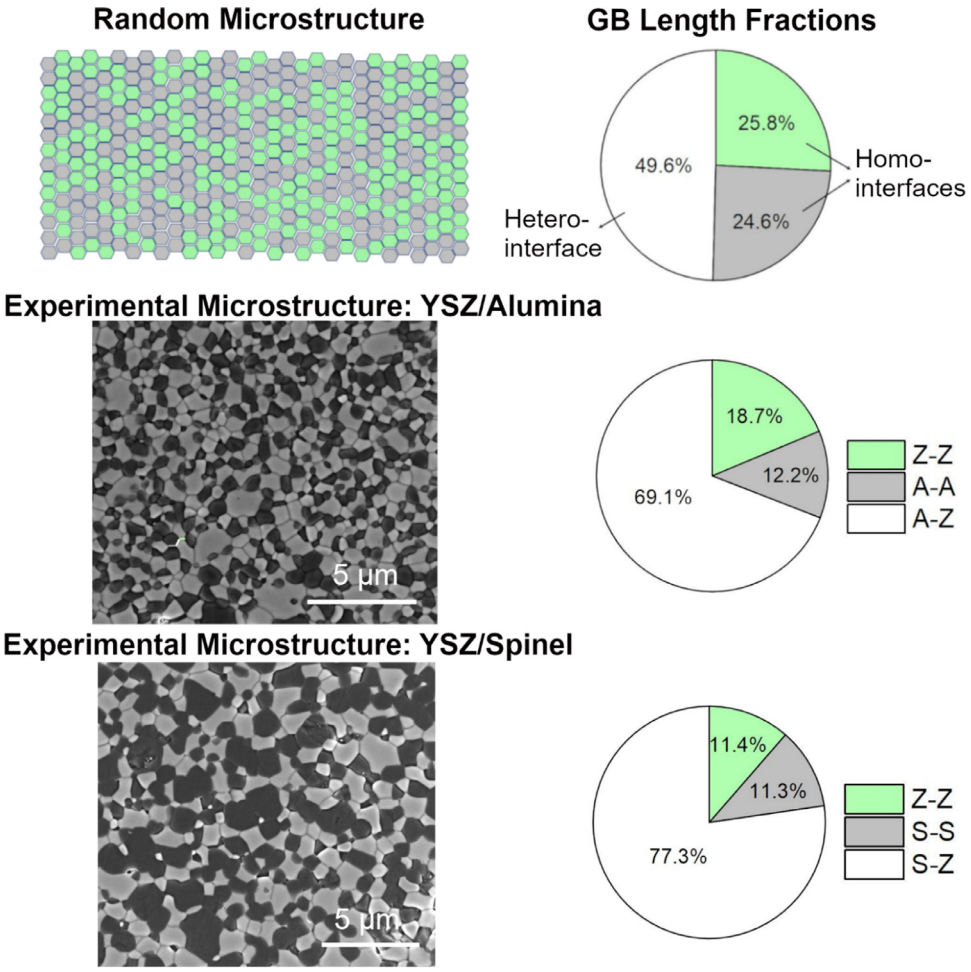

Fig. 8. Calculated grain boundary length fractions in random microstructure of 2-phase composition versus. calculated grain boundary length fractions for YSZ/Alumina and YSZ/Spinel samples. Z=YSZ, S=Spinel, A=Alumina.

terfaces are bound to be in higher fractions in the experimental microstructure when two different phases of equal amounts are homogenously mixed.

For similar sized region in YSZ/spinel, the grain boundary length fractions were calculated to be 11.4% for Z-Z, 11.3% for S-S, and 77.3% for Z-S interfaces (Fig. 8). The average grain boundary energy for Z-Z is 0.9 ± 0.3 J/m^2, S-S is 1.1 ± 0.4 J/m^2, and Z-S is 1.2 ± 0.3 J/m^2 (Table 3). There is direct correlation again seen with very similar average grain boundary energies of Z-Z and S-S interfaces in YSZ/spinel system resulting in similar grain boundary length fractions (Fig. 8). This implies that similar interface energies of Z-Z and S-S in YSZ/spinel result in similar relative interface areas. Again, YSZ/spinel interfaces occur in majority due to both phases mixed homogenously prior to sample pressing. Results from both YSZ/spinel and YSZ/alumina thus confirm the critical role grain boundary energies play in the microstructural development.

4. Conclusion

While the influence of grain boundary energies on microstructural development has been much studied before in single phase polycrystals, our study shows that relative interface areas in multiphase polycrystalline systems are determined by the relative interface energies. We report that alumina-alumina grain boundaries occur less in two-phase YSZ/alumina sample, due to higher grain boundary energy, compared to YSZ-YSZ grain boundaries. Spinel-spinel and YSZ-YSZ grain boundaries occur in similar fractions in YSZ/spinel sample due to similar grain boundary energies. Our results show that variations in grain boundary chemistry in different sample compositions likely affect the energies of boundaries of the same type; however, the changes in average energy values are subtle and can be understood better by looking at energy distribution trends. We also report that Y/Zr segregation to spinel surfaces can stabilize faceting in spinel, while high solubility of Al in spinel increases/worsens the faceting. Lastly, we show that heterointerfaces (YSZ/spinel, YSZ/alumina, spinel/alumina) have intermediate interfacial energies between the grain boundary energies of each of the two parent phases associated with them. The knowledge produced by this work expand the limited existing understanding of interfacial energy measurements in multiphase systems. Thus, this work can serve as a guide towards informed materials design in other technical systems with better understanding about the influence of grain boundary and interfacial energies on microstructure.

Declaration of Competing Interest

The authors declare that they have no known competing financial interests or personal relationships that could have appeared to influence the work reported in this paper.

Acknowledgments

The authors are grateful to Prof. Emerita Martha Mecartney for her feedback in the development of this paper. This work is supported by NSF (DMR 1611457). The authors acknowledge

the use of facilities and instrumentation at the UC Irvine Materials Research Institute (IMRI), which is supported in part by the National Science Foundation through the UC Irvine Materials Research Science and Engineering Center (DMR-2011967). AFM work was performed using an Anton Paar Tosca 400 AFM on loan to IMRI from Anton Paar GmbH. KS acknowledges Somnath Mandal for providing three of the sintered samples used in this study. KS and NM acknowledge additional support from US Department of Education Graduate Assistance in Areas of National Need (GAANN) Fellowships. WJB acknowledges UCI new faculty start-up funding.

Supplementary materials

Supplementary material associated with this article can be found, in the online version, at doi:10.1016/j.actamat.2022.117685.

References

[1] G.S. Rohrer, Grain boundary energy anisotropy: a review, J. Mater. Sci. 46 (2011) 5881–5895.
[2] W.W. Mullins, Two-dimensional motion of idealized grain boundaries, J. Appl. Phys. 27 (1956) 900–904.
[3] S.M. Foiles, Temperature dependence of grain boundary free energy and elastic constants, Scr. Mater. 62 (2010) 231–234.
[4] D. Gupta, Diffusion, solute segregations and interfacial energies in some material: an overview, Interface Sci. 11 (2003) 7–20.
[5] M.N. Kelly, S.A. Bojarski, G.S Rohrer, The temperature dependence of the relative grain-boundary energy of yttria-doped alumina, J. Am. Ceram. Soc. 100 (2017) 783–791.
[6] A. Atkinson, R.I. Taylor, The diffusion of 63Ni along grain boundaries in nickel oxide, Philos. Mag. A 43 (1981) 979–998.
[7] W. Rheinheimer, et al., The equilibrium crystal shape of strontium titanate and its relationship to the grain boundary plane distribution, Acta Mater. 82 (2015) 32–40.
[8] G.S. Rohrer, The role of grain boundary energy in grain boundary complexion transitions, Curr. Opin. Solid State Mater. Sci. 20 (2016) 231–239.
[9] Y. Sato, et al., Role of Pr segregation in acceptor-state formation at ZnO grain boundaries, Phys. Rev. Lett. 97 (2006) 106802.
[10] B. Feng, et al., Atomic structures and oxygen dynamics of CeO_2 grain boundaries, Sci. Rep. (2016), doi:10.1038/srep20288.
[11] S.J. Dillon, M.P. Harmer, G.S Rohrer, The relative energies of normally and abnormally growing grain boundaries in alumina displaying different complexions, J. Am. Ceram. Soc. 93 (2010) 1796–1802.
[12] W.J. Bowman, A. Darbal, P.A. Crozier, Linking macroscopic and nanoscopic ionic conductivity: a semiempirical framework for characterizing grain boundary conductivity in polycrystalline ceramics, ACS Appl. Mater. Interfaces 12 (2020) 507–517.
[13] W.J. Bowman, J. Zhu, R. Sharma, P.A Crozier, Electrical conductivity and grain boundary composition of Gd-doped and Gd/Pr co-doped ceria, Solid State Ion. 272 (2015) 9–17.
[14] D.M. Saylor, G.S Rohrer, Measuring the influence of grain-boundary misorientation on thermal groove geometry in ceramic polycrystals, J. Am. Ceram. Soc. 82 (1999) 1529–1536.
[15] D.M. Saylor, A. Morawiec, G.S Rohrer, The relative free energies of grain boundaries in magnesia as a function of five macroscopic parameters, Acta Mater. 51 (2003) 3675–3686.
[16] N. Shibata, F. Oba, T. Yamamoto, Y. Ikuhara, Structure, energy and solute segregation behaviour of [110] symmetric tilt grain boundaries in yttria-stabilized cubic zirconia, Philos. Mag. 84 (2004) 2381–2415.
[17] H. Yoshida, K. Yokoyama, N. Shibata, Y. Ikuhara, T. Sakuma, High-temperature grain boundary sliding behavior and grain boundary energy in cubic zirconia bicrystals, Acta Mater. 52 (2004) 2349–2357.
[18] A. Tsoga, P. Nikolopoulos, Surface and grain-boundary energies in yttria-stabilized zirconia (YSZ-8 mol%), J. Mater. Sci. 31 (1996) 5409–5413.
[19] S.A. Bojarski, S. Ma, W. Lenthe, M.P. Harmer, G.S Rohrer, Changes in the grain boundary character and energy distributions resulting from a complexion transition in Ca-doped yttria, Metall. Mater. Trans. A 43 (2012) 3532–3538.
[20] H. Vahidi, et al., A review of grain boundary and heterointerface characterization in polycrystalline oxides by (scanning) transmission electron microscopy, Crystals 11 (2021) 878.
[21] K. Syed, et al., Correlations of grain boundary segregation to sintering techniques in a three-phase ceramic, Materialia (2020) 100890, doi:10.1016/j.mtla.2020.100890.
[22] S.J. Dillon, M.P. Harmer, G.S Rohrer, Influence of interface energies on solute partitioning mechanisms in doped aluminas, Acta Mater. 58 (2010) 5097–5108.
[23] P. Haremski, et al., A thermal grooving study of relative grain boundary energies of nickel in polycrystalline Ni and in a Ni/YSZ anode measured by atomic force microscopy, Acta Mater. 214 (2021) 116936.
[24] N.E. Munoz, S.R. Gilliss, C.B. Carter, The monitoring of grain-boundary grooves in alumina, Philos. Mag. Lett. 84 (2004) 21–26.
[25] W.W. Mullins, Theory of thermal grooving, J. Appl. Phys. 28 (1957) 333–339.
[26] W.M. Robertson, Grain-boundary grooving by surface diffusion for finite surface slopes, J. Appl. Phys. 42 (1971) 463–467.
[27] C.A. Handwerker, J.M. Dynys, R.M. Cannon, R.L. Coble, Dihedral angles in magnesia and alumina: distributions from surface thermal grooves, J. Am. Ceram. Soc. 73 (1990) 1371–1377.
[28] G.C.C. Costa, S.V. Ushakov, R.H.R. Castro, A. Navrotsky, R. Muccillo, Calorimetric measurement of surface and interface enthalpies of Yttria-Stabilized Zirconia (YSZ), Chem. Mater. 22 (2010) 2937–2945.
[29] J.M. McHale, A. Auroux, A.J. Perrotta, A. Navrotsky, Surface energies and thermodynamic phase stability in nanocrystalline aluminas, Science 277 (1997) 788–791.
[30] M.M. Hasan, et al., Improving the thermodynamic stability of aluminate spinel nanoparticles with rare earths, Chem. Mater. 28 (2016) 5163–5171.
[31] J. Teevan The Effect of Titanium Dioxide Doping On Th Grain Growth and Grain-Boundary Energy of Magnesium Aluminate Spinel. (Lehigh University).
[32] J.R. Heffelfinger, M.W. Bench, C.B Carter, On the faceting of ceramic surfaces, Surf. Sci. 343 (1995) L1161–L1166.
[33] B. Ratzker, M. Sokol, S. Kalabukhov, N. Frage, Creep of polycrystalline magnesium aluminate spinel studied by an SPS apparatus, Materials 9 (2016) 493 (Basel).
[34] Y.K. Simpson, C.B Carter, Faceting behavior of alumina in the presence of a glass, J. Am. Ceram. Soc. 73 (1990) 2391–2398.
[35] S.K. Mohan, R. Sarkar, Effect of ZrO_2 addition on $MgAl_2O_4$ spinel from commercial grade oxide reactants, Ceram. Int. 42 (2016) 10355–10365.
[36] A.P. Tomsia, A.M. Glaeser, Ceramic Microstructures: Control at the Atomic Level, Springer Science & Business Media, 2012.
[37] B. Hallstedt, Thermodynamic assessment of the system MgO–Al_2O_3, J. Am. Ceram. Soc. 75 (1992) 1497–1507.
[38] B. Feng, N.R. Lugg, A. Kumamoto, Y. Ikuhara, N. Shibata, Direct observation of oxygen vacancy distribution across yttria-stabilized zirconia grain boundaries, ACS Nano 11 (2017) 11376–11382.
[39] K. Matsui, H. Yoshida, Y. Ikuhara, Grain-boundary structure and microstructure development mechanism in 2–8mol% yttria-stabilized zirconia polycrystals, Acta Mater. 56 (2008) 1315–1325.
[40] G. Sánchez-Santolino, et al., Localization of yttrium segregation within YSZ grain boundary dislocation cores, Phys. Status Solidi A 215 (2018) 1800349.
[41] R.D. Shannon, Revised effective ionic radii and systematic studies of interatomic distances in halides and chalcogenides, Acta Crystallogr. A 32 (1976) 751–767.